Journal of Metals, Materials and Minerals, 34(1), 1855, 2024

Investigating the high-impact deformation behavior of induced-nano precipitation hardened in718 alloy

Harrison Okechukwu ONOVO[1,*], Muideen Adebayo BODUDE[1], David Ehigie ESEZOBOR[1], and Thaddeus Tochukwu AKANO[2]

[1] *Department of Metallurgical and Materials Engineering, University of Lagos, Akoka, Yaba, Lagos Mainland, Lagos, 101017, Nigeria*
[2] *Deparment of Mechanical Engineering, University of Botswana, Gaborone, UB 0022, Botswana*

***Corresponding author e-mail**: honovo@unilag.edu.ng

Received date:
28 September 2023
Revised date
31 January 2024
Accepted date:
13 March 2024

Keywords:
Dynamic impact;
Flow stress;
Hopkinson pressure bar;
Strain rate;
Superalloy

Abstract

Superalloys are the preferred materials for modern high-rotational complex components due to their exceptional ability to maintain critical properties such as strength, oxidation/corrosion resistance, even under extreme temperatures and dynamic impacts. This study investigates the dynamic impact response of nanoprecipitation-hardened 718 alloy (NPH-718 alloy) under various loading conditions. The wrought nickel-based NPH-718 alloy was transformed into a nanostructured state through a precise heat treatment process involving controlled cooling rates (28°C·s^{-1} to 30°C·s^{-1}). A mechanical compression test, leading to failure, was employed to assess the alloy's ability to withstand dynamic impacts. The compressive dynamic behavior of the alloy at high strain rates (4000 s^{-1} to 7500 s^{-1}) and temperatures ranging from –180°C to 750°C was evaluated using a custom-built direct impact Hopkinson pressure bar apparatus. The flow data obtained for NPH-718 alloy exhibited sensitivity to thermally activated processes. Consequently, as the temperature increased at a constant high loading rate, both flow stress and adiabatic effect increased. Conversely, at a constant deformation temperature, the flow characteristics exhibited an increase as the loading rate decreased. This study establishes key trends in the flow stress, adiabatic effect, temperature, and the strain rate sensitivities of NPH-718 alloy, offering valuable insights for design and performance evaluation purposes. It underscores the significant influence of temperature and strain rate on the flow behavior of NPH-718 alloy, further solidifying its reliability in demanding applications.

1. Introduction

Design and service performance evaluation of complex modern components in high rotational services necessitates in-depth knowledge of material performance enhancement parameters at low and high temperatures. Most material's performance enhancement parameters differ with varying processing techniques such as high rate of loading, deformation history, and deformation temperature. Unfortunately, these changes in materials processing parameters often lead to significant variations in critical properties of materials such as strength, and have increased the need for comprehensive investigation and understanding of high-speed (supersonic) deformation behaviour of exceptionally high temperature materials such as novel nanoprecipitation hardened 718 alloy (NPH-718 alloy) superalloys. The NPH-718 alloy is a gamma double prime (γ^{II}) precipitation hardened nickel-base superalloy, widely used in high temperature zone and as complex rotating components in aerospace and industrial turbine engines since its development around the 1940s [1]. NPH-718 alloy has an exceptional balance of properties at changing temperature conditions, making it an attractive material for complex rotating components of various classes of turbines.

The behaviour of high temperature alloys under low-rate (<10^3 s^{-1}) dynamic deformation has been widely reported [2-4], but very few published works have been documented in the literature concerning the deformation behaviour, which underscores little understanding of the high dynamic rate of loading (>10^3 s^{-1}), temperature, and deformation history of NPH-718 alloy. Temperature and strain rate have the greatest effects on the NPH-718 alloy's fast dynamic deformation rate [5]. There is a growing need for a thorough investigation of this alloy's plastic behaviour and dynamic impact properties across a broad spectrum of important deformation factors, including strain, deformation temperature, and strain rate. This is because this alloy meets requirements for high-temperature critical applications.

The Split Hopkinson Pressure Bar (SHPB) system is the principal technique for examining materials' flow characteristics under high impact deformations. This technique was employed to test materials' dynamic impact response to high strain rate deformation in order of 10^2 s^{-1} to 10^4 s^{-1} [6-8]. The mechanical properties of composites and other non-metallic materials evaluated through the SHPB procedures at varied deformation conditions: temperatures and strain rates have shown a substantial modification of properties. Thermal activation [9] as well as dislocation damping [10], are among the suggested

leading mechanisms that could cause the inevitable vicissitudes in the mechanical properties of materials.

Consequently, the extensive temperature- and strain-rate-reliant research are necessary to understand fully the mechanical behaviours of engineering materials with respect to the fundamentally important dynamic impact deformation parameters of strain, strain rate, and temperature [11]. Moreso, depending on the specimen's properties such as strength, dimensions, and deformation loading conditions, the strain rates of about 5×10^2 s^{-1} to 8×10^3 s^{-1} are typically attained in turbine applications. Thus far, literature has some publications that unveiled the dependence of flow stress of engineering materials, for instance, titanium and copper on deformation parameters and links the relationship directly to microstructural evolutions resulting from high-loading deformations [12,13]. Consequently, the DI-SHPB compressive deformation technique is adapted for a holistic evaluation of NPH-718 alloy dynamic impact response at different extreme deformation conditions of temperatures extending from –180°C to 750°C in addition to strain rates that start from 4×10^3 s^{-1} to 7.5×10^3 s^{-1}. The state-of-art metallographic techniques such as optical microscopy, scanning microscopy, and high-resolution transmission microscopy were adopted for observation and analysis of the evolving micro-structures, which assisted the discussions on varying mechanical behaviours of the dynamically deformed samples at different deformation parameters. This study, therefore, presents exhaustive actualities and informative characteristics of dynamic impact response together with microstructural evolutions of NPH-718 alloy at extreme temperatures and strain rates feasible in real engineering applications. Applications of this alloy abound and cut across turbines, and other critical equipment for pollution control, and storage containers at cryogenic conditions, to mention a few.

2. Materials and methods

2.1 Material preparation

The 718 alloy employed in this research was obtained in the form of a solid wrought plate measuring 2 cm × 12 cm × 40 cm, sourced from the Department of Mechanical Engineering at the University of Manitoba, Canada. The compositional analysis of the alloy was conducted using the SEM-EDS facility. The cylindrical specimens were sectioned out from the as-received wrought alloy in conformity to the relation in Equation (1), where L, D and v are the specimen length, diameter and the Poisson's ratio respectively.

$$\frac{L}{D} = \sqrt{\frac{3v}{4}} \tag{1}$$

To limit the tendency of buckling during the dynamic compression tests, the length-to-diameter ratio of the cylindrical specimen was chosen to be approximately 0.9 [14]. The samples were machined to a predefined solid cylindrical shape a with diameter of 9.5 mm and length of 10.5 mm, using Hansvedt EDM Model DS2/20 serial AJ23101 Traveling Wire Electrical Discharge Machine. The faces of the specimen are parallel and flat with good precision.

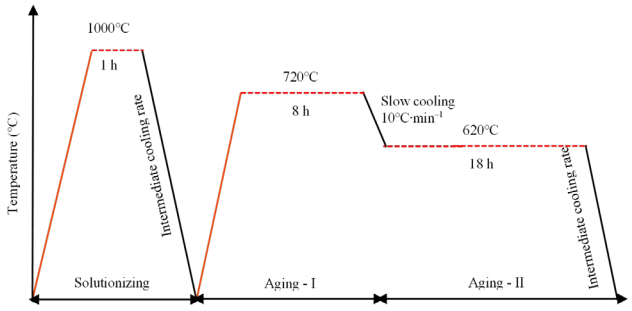

Figure 1. Heat treatment conditions used for synthesis of NPH-718 alloy.

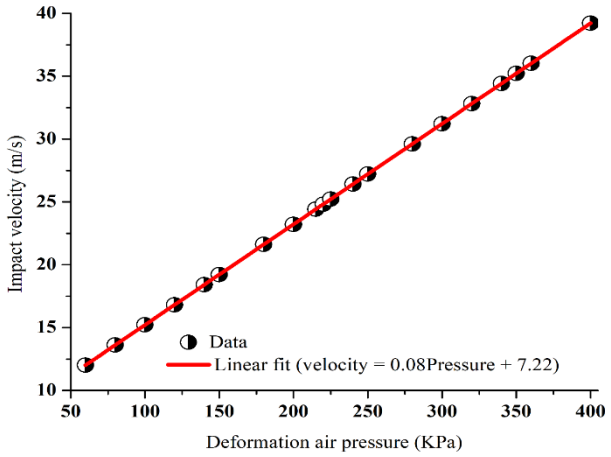

Figure 2. The linear relationship existing between impact velocity and firing pressure.

2.2 Development of nano precipitates structured 718alloy

Precipitated particles are the most significant hardening particles in superalloys, which has their sizes in their normal condition above the nanoscale. Exceptional properties of metallic alloys are realized when the materials' particulate sizes are on the nanoscale. To tailor nano-precipitated particles in superalloys to nanostructure, it has been reported that three factors that affect the formation of particles in superalloys must be effectively controlled. These include temperature, soaking period, and cooling rate [15]. Figure 1 shows the thermal procedural schedule for the formation of the nanoprecipitation structure of 718 alloy and some thermally processed samples. Lengthy thermal (Solutionization, Stabilization and precipitation hardening) treatments, various thermal cooling processes were employed, spanning a range of 0.25°C·s^{-1} to 500°C·s^{-1}, along with different soaking durations, to facilitate the development of nano-precipitates in 718 alloy super-alloys. Nano-precipitates were achieved at the cooling rate of around 28°C·s^{-1} to 30°C·s^{-1} in 718 alloy. Accordingly, any divergence from the aforementioned practises and conditions will result in adverse results.

2.3 Impact velocity and firing air pressure

When the gun is released to fire, the striker bar strikes or impacts the specimen at a predetermine velocity. As a result of the impact loading or deformation on the specimen, elastic waves are generated

and propagate through the specimen towards the transmitter bar, which is affixed to the momentum catcher. Oscilloscope is used to capture the amplified elastic waves which are recorded in terms of voltage (mV) – time (microsecond) data. The impact velocity of the striker bar has a direct relationship with the firing pressure as expressed in Equation (2) which agrees with the impact velocity of Delorme, [16] and the correlation between the two impact momentum parameters (impact velocity and firing pressure) with a high degree of approximation is presented in Figure (2).

$$\text{Impact velocity} = 0.08*\text{striker bar pressure} + 7.22 \quad (2)$$

2.4 High strain rate deformation of NPH-718 alloy

This work used the direct impact pressure bar technology (DI-SHPB), housed in the department of mechanical engineering, University of Manitoba, Canada, to achieve dynamic impact deformation under varied deformation temperatures. Both high and low deformation temperatures are included in the approach. Typically, to retain the specimens in contact with the transmitted bar at low deformation temperatures, a small coating of very viscous grease is applied to the interface between the specimen and the transmitted bar. For high-temperature tests, there is an integration of a customized furnace structure that can heat the specimens up to 1200°C. The implemented heating system contains a proportional integral derivative (PID) control which is used to adjust the temperature level as well as programmable heat treatment schedules such as soaking stages. The programmable feature helps to make certain that the temperature control is uniform, and the timing is regular for all the specimens. Similarly, the ancillary feature or device that hold the specimen is instituted. It takes the sample inside the furnace during heating processes and brings it out for impact test after heating within a predetermined time.

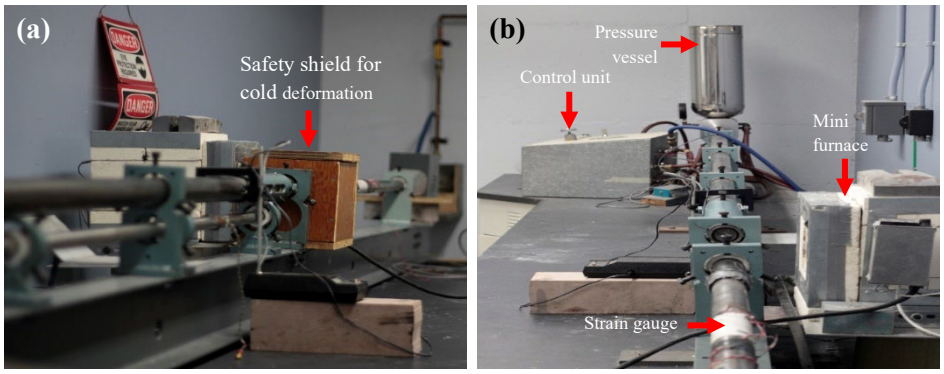

Figure 3. Low and hot deformation components of DI-SHPB setup with: (a) wooden safety shield for low temperature, (b) custom built mini furnace, pressure vessel and control unit, for hot impact test at the University of Manitoba, Canada.

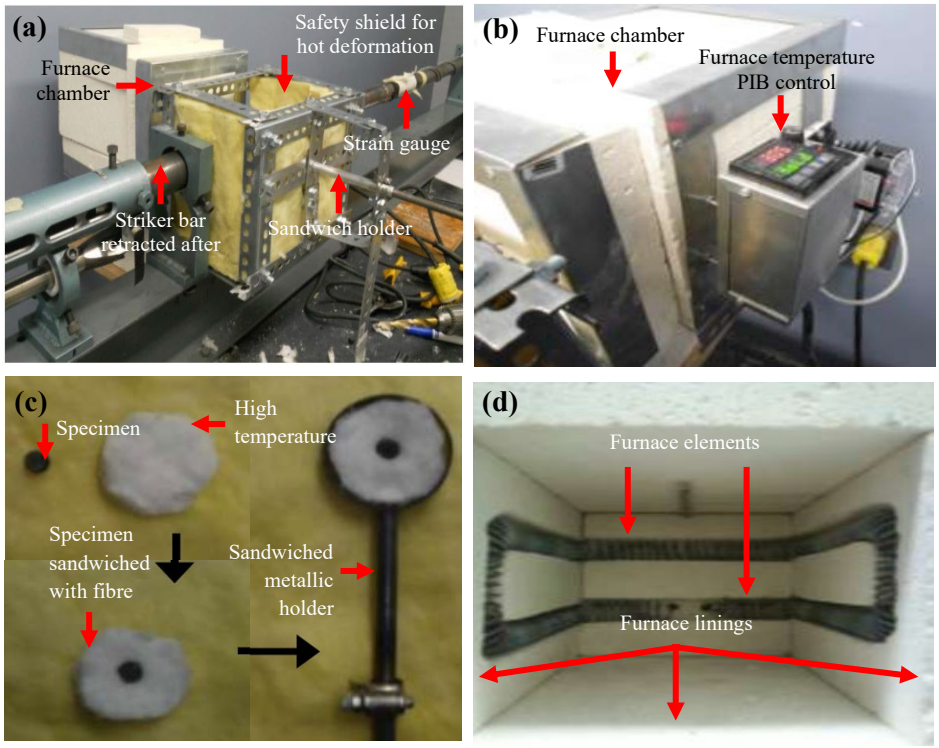

Figure 4. Low and hot deformation components of DI-SHPB setup with: (a) fibre safety shield for high temperature, (b) furnace exterior with PIB control box, (c) sandwich holder makeup, and (d) furnace interior for hot impact test at the University of Manitoba, Canada.

For safety purposes, a wooden safety box is used for low-temperature deformation while a fiber sandwich and a metallic frame holder were effectively used to grip the specimen and take it in and out of the furnace for impact eformations at high temperature as shown in Figure 3(a-b) and Figure 4(a-d). The cryogenic deformation temperature of –180°C was achieved through a refrigeration system [17]. The refrigeration system was formed with stryofoam cold chamber, filled with oxygen and liquid nitrogen. The liquid nitrogen completely covered up the specimen to reach a predetermined cryogenic testing temperature. The specimen temperature was tracked using a K-type thermocouple operated at the sampling rate of 1Hz [18].

Direct impact tests were conducted on NPH-718 alloy specimens, under the deformation temperatures of –180°C, 25°C, 300°C, 550°C, 650°C, and 750°C. For each deformation temperature, the specimens were deformed at four different air pressures: 200 kPa, 250 kPa, 300 kPa, and 350 kPa corresponding to impact velocities of 23 $m{\cdot}s^{-1}$, 27 $m{\cdot}s^{-1}$, 31 $m{\cdot}s^{-1}$, and 35 $m{\cdot}s^{-1}$ respectively. The high temperature was achieved using a heating unit while the cold deformation was done through liquid nitrogen.

3. Results and discussion

3.1 Elemental composition

This study implemented dynamic impact deformation test using nickel-based NPH-718 alloy with elemental composition (weight) of Cr 21.02%, Co 13.50%, Ti 3.12%, Al 1.74%, O_2 0.61% and the balance is Ni 60.01%.

3.2 Microstructure examination

The optical microscopic analysis of the NPH-718 alloy subjected to high strain rates ($6 \times 10^3 s^{-1}$) and extreme temperature conditions, both at frigid (–180°C) and ambient room temperatures (25°C), is illustrated in Figure 5(a-b). This examination unveiled the presence of densely clustered dislocations and substructures exhibiting characteristics akin to straight annealing twins' lamellae. Furthermore, scanning electron microscopy, as demonstrated in Figure 6(a-b), provided additional insights into the material's microstructure, revealing the existence of deformation shear bands and intermetallic compounds. To comprehensively investigate the formation of nanostructured precipitates within the NPH-718 alloy, a detailed examination was conducted using a transmission electron microscope (TEM). This examination included a comprehensive assessment of the selected area diffraction pattern (SADP). The TEM SADP analysis definitively corroborated the presence of precipitation particles within the NPH-718 alloy, elucidating their distinctive patterns and arrangements.

The diffraction patterns obtained from this analysis were meticulously scrutinized, ultimately revealing the 112 diffraction patterns characteristic of the NPH-718 alloy's gamma double prime (γ") phase, as illustrated in Figure 7. Furthermore, the micrographs of the NPH-718 alloy were instrumental in elucidating the material's structures and delineating the range of particle sizes, as depicted in Figure 8. Through meticulous TEM examination, it was ascertained that the precipitate particle sizes fell within the nanometer scale, with an approximate size of 19 nm.

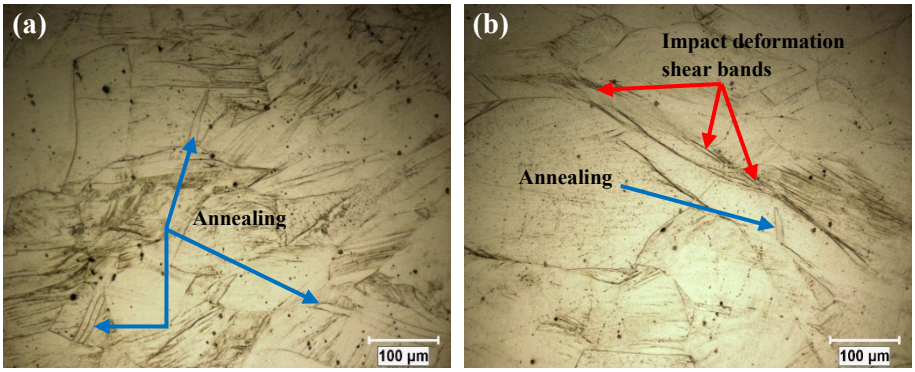

Figure 5. Optical micrographs of NPH-718 alloy impacted at constant $\dot{\varepsilon}$ 6×10^3 s^{-1}: (a) –180°C, and (b) 25°C.

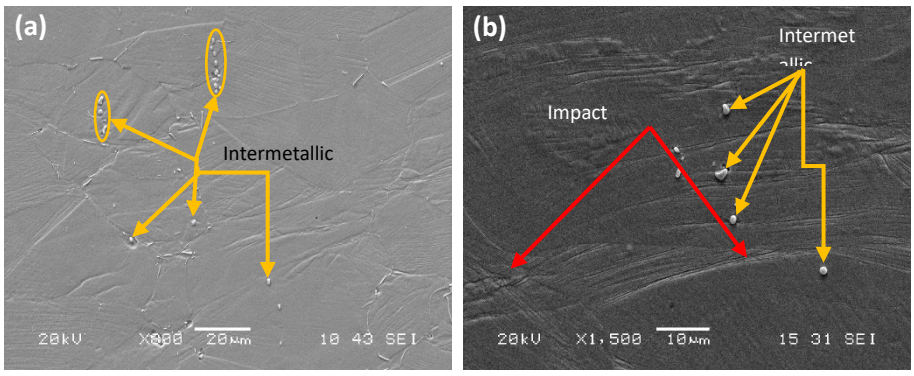

Figure 6. Scanning electron micrograph for NPH-718 alloy impacted at constant $\dot{\varepsilon}$ 6×10^3 s^{-1}: (a) –180°C, and (b) 25°C.

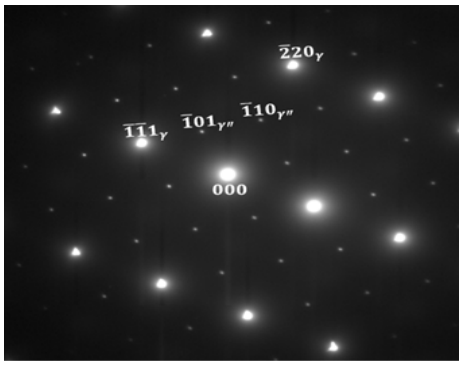

Figure 7. SADP image of transmission electron for NPH-718 alloy (γ'')

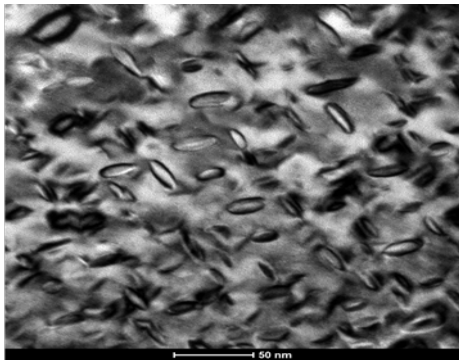

Figure 8. Transmission electron micrograph for NPH-718 alloy (γ'').

3.3 Analysis of materials deformation behaviour (flow stress-strain) of NPH-718 alloy

The dynamic impact response of the nanostructured precipitation-hardened 718 alloys subjected to varying strain rates, ranging from $4 \times 10^3\ s^{-1}$ to $7.5 \times 10^3\ s^{-1}$, and temperatures spanning from –180°C to 750°C, is meticulously documented in Figure 9(a-d). It is discernible that the interplay between deformation temperature and strain rate in NPH-718 alloy exerts a profound influence on the material's flow behavior during dynamic deformation scenarios. In the context of dynamic loading conditions, the flow stress experiences a rapid surge at the inception of dynamic plastic deformation or at low strain levels, subsequently intensifying as deformation progresses. This conspicuous augmentation in flow stress observed during the initial stages of impact deformation can be attributed to multiple factors, including an augmented dislocation density and the genesis and expansion of sub-grain boundaries. These phenomena are likely consequences of deformation mechanisms encompassing work hardening and dynamic recovery processes [19].

Furthermore, it is noteworthy that as the magnitude of strain increases, the flow stress value undergoes a decline after reaching its pinnacle. This decline in flow stress is a result of the strain and strain rate hardening effects being outweighed by the thermal softening effect induced by the heat generated during dynamic plastic deformation [20].

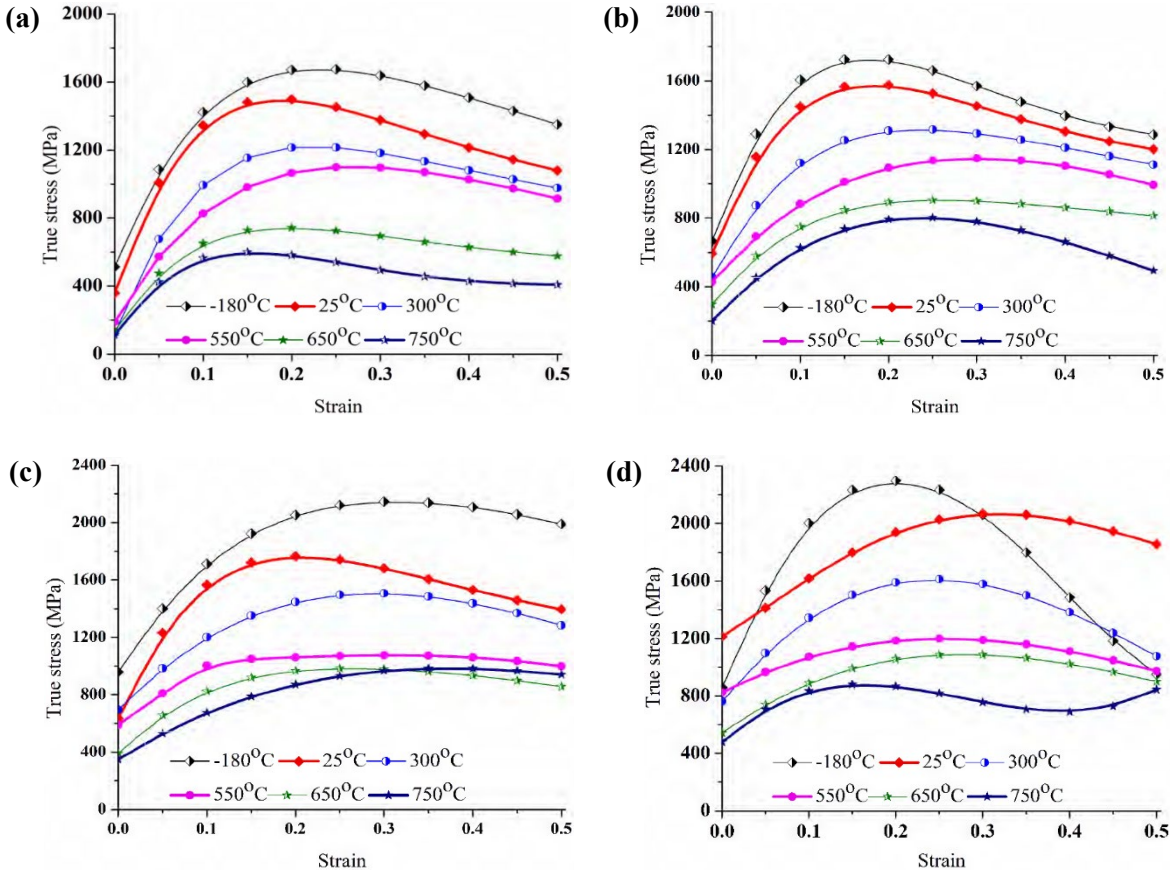

Figure 9. NPH-718 alloy (a, b. c and d) deformed at constant strain rates, different temperatures (–180°C to 750°C) and strain (0 to 0.5).

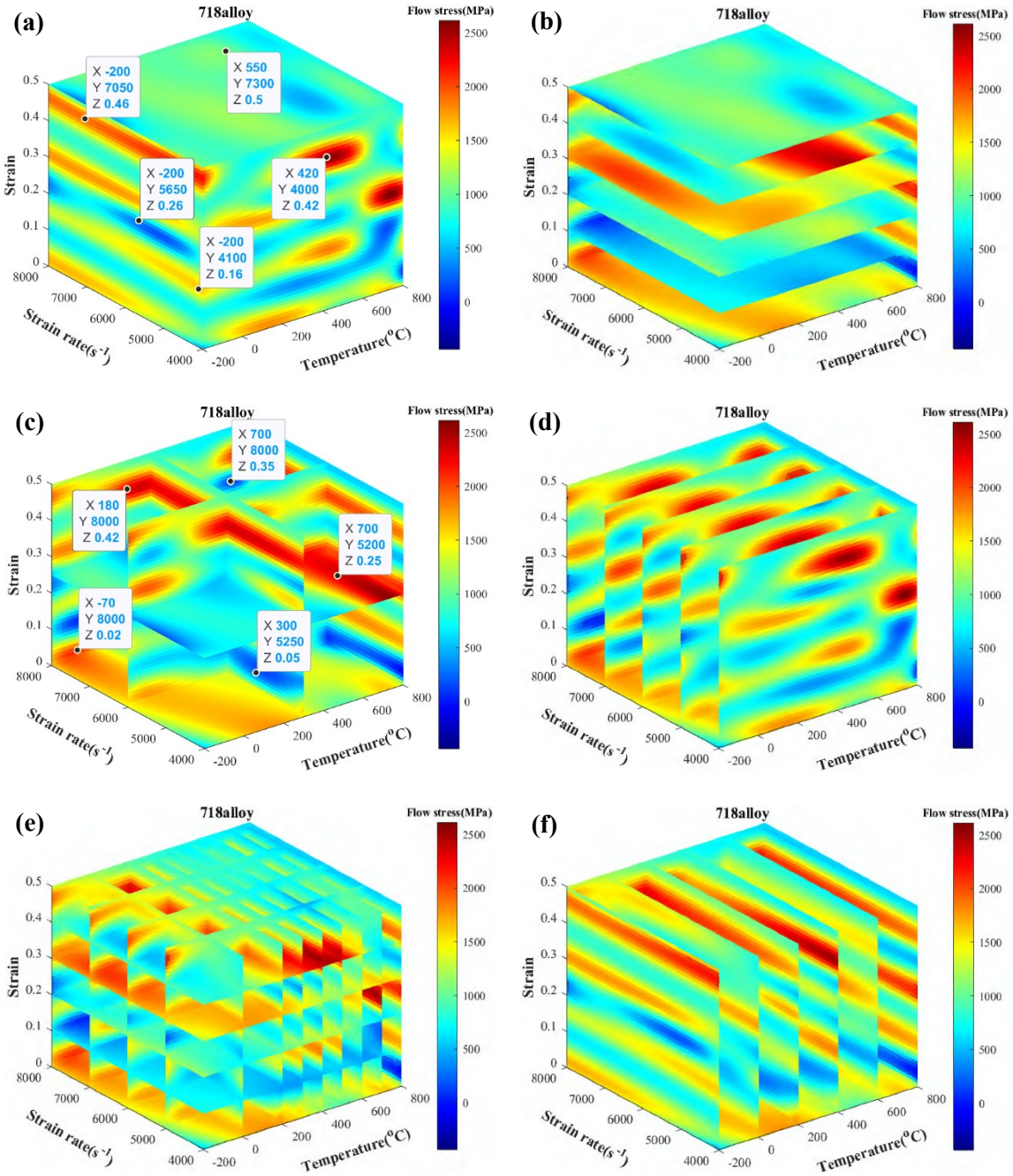

Figure 10. Stress map of NPH-718 alloy in 3D blocks: all parameters are visible in (a); strain, strain rate, and deformation temperature are fixed in (b) and (c); strain, strain rate, and deformation temperature are fixed for (d), (e), and (f), respectively.

3.4 NPH-718 alloy dynamic behavior on 3D-map

To delve deeper into the ongoing link between deformation parameters, specifically deformation temperature, strain, and strain rate, associated with deformations that occurs with a spilt second, the emerging innovative procedures of data mapping or charting will be ultraconvenient. Data mapping ensures an uncondensed illustrative examination of the continuous correlation of influential deformation parameters. Categorically, 2D and 3D mappings are feasible. As 3D mapping will enable the descriptive analysis of two parameters while keeping the other constant, the 2D will only allow for effective study of two parameters pictorially.

The examination of a 2D contour plot depicting deformation temperature and strain rate was the first data mapping in the field of plastic deformation. This study proved the direct relationship between deformation temperature and strain rate sensitivity, as well as the fact that strain rate varies inversely with strain rate sensitivity [21]. In lieu, a rhombus data matrix was adapted to implement 3D mapping on a steady deformation condition with varied deformation parameters: stress, strain rate, temperature, and strain [22], which was later reexamined to be defective by reason of stress, a resultant descriptive effect of deformation being considered an input parameter in plastic deformation. This review and uncovering in the maiden 3D data mapping report led the first suitable data mapping in 3D

implemented on stress data of Ti-6Al-2Zr-1Mo-1V alloy with diverse strains, strain rates and temperatures [23]. Moreover, very suitable 3D data mapping has also been implemented on dynamically deformed nickel-based waspaloy to further examine the effect of flow stress, strain, deformation temperature, and strain rate [23].

Likewise, this study adapts pertinent 3D data mapping for more examination of NPH-718 alloy flow stress data obtained from high strain rate impact deformation. Unlike the 2D deformation data mapping, the 3D maps resultant deformation flow stress data with varied avails the interpolation window to populate the experiential response data for exhaustively investigation.

The flow stress data of NPH-718 alloy is interpretable in 3D axis (x, y, and z) block (Figure 10(a)) without varying any parameter. Figure 10(b) unveils the flow stress distributions in the inward slice of 3D color block, revealing the deformation response graduation in its intensity from the lower to higher levels of the parameters. In the same way, the flow stress data can further be scrutinized by fixing significant deformation parameters (strain, deformation temperature, and strain rate) constant (Figure 10(c)), providing a closer view of deformation parameters for easy valuation.

At constant strain, the strain rate and deformation temperatures effects were shown in Figure 10(d) which additionally confirms strain value of 0.3 to be approximate the onset of peak flow stress. Also, Figure 10(e) avails the possibility to examine the activities of strain as well as deformation temperatures when strain rate is kept constant wherein the progression of flow shades of colorations on a color bar while the influential deformation parameters are put side by side on gradation 3D block. More importantly, 3D deformation data mapping also stress as strain increases is evident. Moreso, holding deformation temperatures constant enables the investigation into the effect of strain and strain rate on the deformation properties of NPH-718 alloy confirms the fact that flow stress rises with increased cooling during deformation [23]. Obviously, charting NPH-718 alloy deformation behavior at varied deformation conditions implemented in this study yields a more descriptive and enhanced analysis owing to an increased volume of available data.

3.5 Effect of thermal softening (adiabatic) on plastic behaviour of NPH-718 alloy

The thermal disposition of NPH-718 alloy, which includes inherent thermal conductivity and high dynamic strain rate, is directly related to the various influencing parameters on plastic flow behavior, which are attributed to the effects of adiabatic softening. As a result, during low-velocity deformation testing under isothermal circumstances, the heat created in the process has adequate time to seep into the environment, having little or no influence on the total temperatures of the NPH-718 alloys.

At high dynamic loading rates, on the other hand, deformations happen so fast (in fractions of a second) that the heat generated by resistance to particle/grain movement through uneven particles does not have enough time to disperse to the environment. This impediment to heat transport unavoidably results in an artificial heat trap inside the sample, which influences the material's deformation behaviour. Furthermore, during the plastic deformation of materials, the majority (up to 90%) of the work done on a sample is converted into heat [24]. This phenomenal test condition called the adiabatic heating condition, is responsible for the material's thermal softening [25]. The Taylor-Quinney connection [26], which is illustrated in Equation (3), expresses the influence of temperature rise during plastic deformation.

$$\Delta T = \frac{\beta}{\rho \times C_p} \int_0^{\varepsilon} \sigma \times d\varepsilon \tag{2}$$

Where ΔT (°C), C_p (J·g^{-1}·°C^{-1}), ρ (kg·m^{-1}), σ (MPa) and ε are the rise in temperature of the specimen during the deformation, specific heat, density, axial true stress, as well as the axial plastic strain. The integral function, β of Equation (2) denotes the plastic (total) work done. It is represented by the integral function of Equation (2), which considers the proportion of overall plastic work transferred into heat during deformation, with a conventional value of 0.9. According to MacDougall [25], the amount of work turned into heat is heavily influenced by the material's stress and alloying components. Thermal softening effects are detrimental and affect the work hardening ability of the material [25].

However, it is problematic to measure the rise in temperature during high-speed deformation conditions, hence approximate calculations using Equation (3) is relied on to deduce the temperature rise, ΔT during plastic deformation [5]. The density, ρ of NPH-718 alloy is approximately 8.22 (g·cm^{-3}), with a 435 (J·g^{-1}·°C^{-1}), C_p heat capacity. Additionally, flow stress represents the stress σ, whereas the strain interval, $d\varepsilon$ is the corresponding true strain. Figure 11 shows the variation in temperature increase during deformation relating to strain, deformation temperature, and the rate of strain. As the temperature rise, ΔT increases, and the strain rate increases. However, when it comes to temperature, it shows a reverse trend. For all loading conditions and the superalloys examined, the maximum thermal softening or rise in temperature consequence in the affected sample is observed at the highest strain rate (7.5×10^3 s^{-1}) but at the lowest temperature (–180°C). Similar trend occurs in the flow stress-strain characteristics of IN 718 as contained in Figure 9(a-d). It is evident that the latter recorded higher temperature rise, ΔT when benchmarked with Waspaloy of [23], almost in all the dynamic impact conditions.

3.6 Rate of strain hardening

The plastic deformation characteristics of numerous metals can be effectively elucidated through the application of the power law equation, as denoted by Equation (4):

$$\sigma = k\varepsilon^n \tag{4}$$

In this equation, k signifies the strength coefficient, while n embodies the empirical constant or work-hardening exponent. It is important to emphasize that Equation (4) does not possess inherent fundamental significance. Typically, deviations from the relationship described by Equation (4) manifest either at low strains ($\varepsilon = 10^{-3}$) or at high strains ($\varepsilon \gg 1.0$). However, when experimental data conform to Equation (4), a log-log or ln-ln representation of the true stress-strain relationship spanning from the initial load or stress to the utmost point will not yield a curved trajectory but instead a

linear one. The work-hardening exponent, n, finds its representation in the slope of this linear correlation, while the strength coefficient, K, corresponds to the true stress at a plastic strain of $\varepsilon = 1.0$. It is essential to underscore that the rate of strain hardening or work hardening in a material, denoted as $\frac{d\sigma}{d\varepsilon}$, exhibits distinct characteristics from the strain-hardening or work-hardening exponent, symbolized as n. The connection between these two parameters is derived from the definition of n as articulated in Equation (5):

$$n = \frac{d(In\ \sigma)}{d(In\ \varepsilon)} = \frac{d(log\ \sigma)}{d(log\ \varepsilon)} = \frac{d\sigma}{d\varepsilon} \times \frac{\sigma}{\varepsilon} \quad (5)$$

$$hence, \quad \frac{d\sigma}{d\varepsilon} = n\,\frac{\sigma}{\varepsilon} \quad (6)$$

In this investigation, the gradient of the flow stress-strain curve, resembling a log-log plot, serves as a fundamental tool for determining the empirical constants denoted as n. These constants, n, play a pivotal role in the computation of work-hardening rates. The flow stress-strain relationship consistently exhibits work-hardening trends in graphical representations across diverse dynamic deformation scenarios.

Figure 12(a-d) present a comprehensive depiction of the work-hardening rates ($\partial\sigma/\partial\varepsilon$) under various deformation conditions, spanning a wide spectrum of temperatures (–180°C to 750°C), true strains ranging from 0.1 to 0.5, and a diverse range of strain rates, extending from 4×10^3 s^{-1} to 7.5×10^3 s^{-1}. These empirical constants, n, employed to quantify work-hardening rates, are extracted from the gradient of the flow stress-strain curve, which fundamentally constitutes a log-log plot. Notably, graphical representations of the flow stress-strain relationship under varying dynamic deformation conditions consistently reveal distinct work-hardening tendencies. A salient observation from these figures is the discernible variation in work-hardening rate $\frac{\partial\sigma}{\partial\varepsilon}$ ontingent upon the specific deformation parameters, including strain, strain rate, and temperature. It is readily apparent that the most pronounced work hardening effect, as documented in this study, manifests under conditions characterized by the lowest deformation temperature (–180°C), the narrowest strain range (approximately 0.2), and the highest strain rate (7.5×10^3 s^{-1}). At a given strain rate, the work hardening rate of the NPH-718 alloy exhibits a decrease with increasing strain and temperature, a phenomenon elucidated in Figure 12(a-d)

Furthermore, it is worth noting that, under fixed temperature and strain conditions, the strain hardening rate registers an increase as the strain rate escalates. This observation underscores the profound influence of temperature on strain rate sensitivity, accentuating the thermal softening effect as a consequence of elevated temperatures during dynamic impact deformation. Importantly, the dynamic work hardening effect emerges as the dominant mechanism, eclipsing the thermal softening effect within the NPH-718 alloy. Notably, the studied NPH-718 alloy demonstrates a capacity for undergoing stable dynamic plastic deformation even under conditions characterized by high temperatures and significant loading forces.

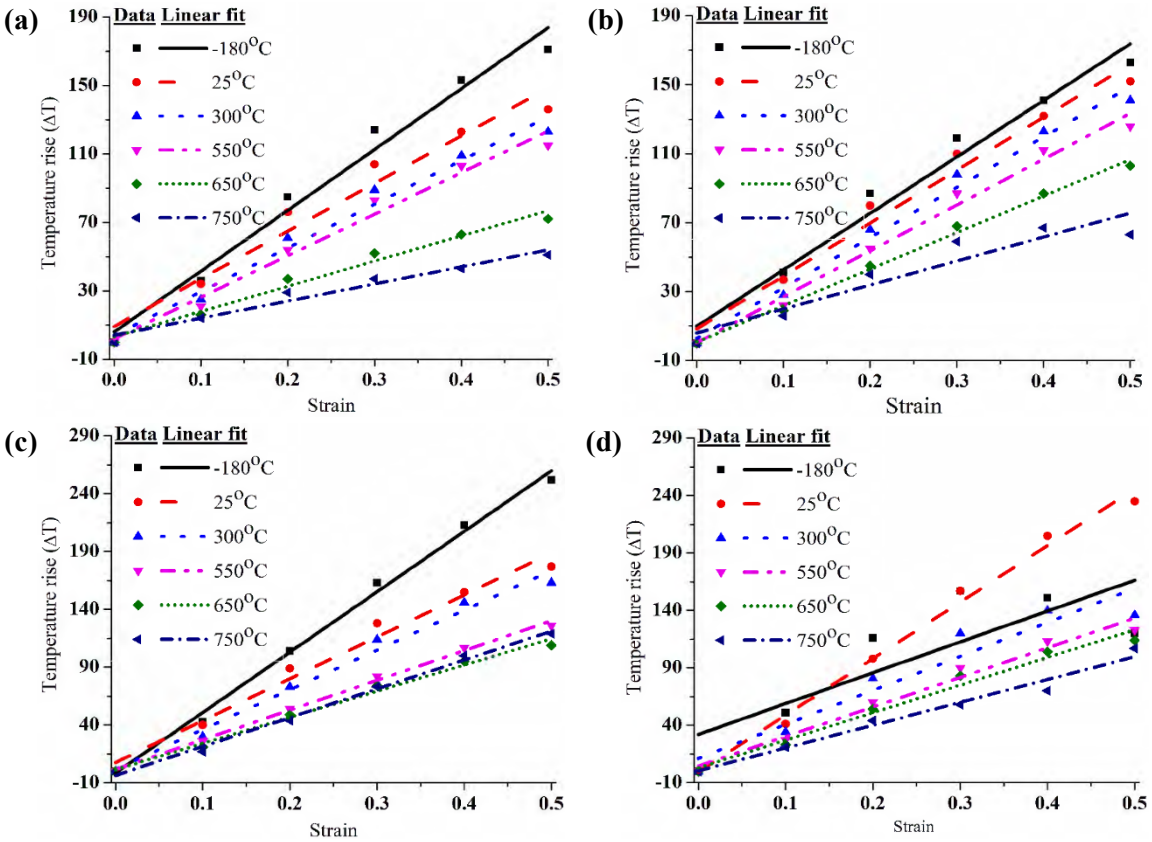

Figure 11. The increase in temperature, ΔT, occurring during the process of plastic deformation of NPH-718 alloy at fixed strain, diverse strain rates 4000 s^{-1} (a), 5000 s^{-1} (b), 6000 s^{-1} (c), and 7500 s^{-1} (d), and various deformation temperatures from –180°C to 750°C.

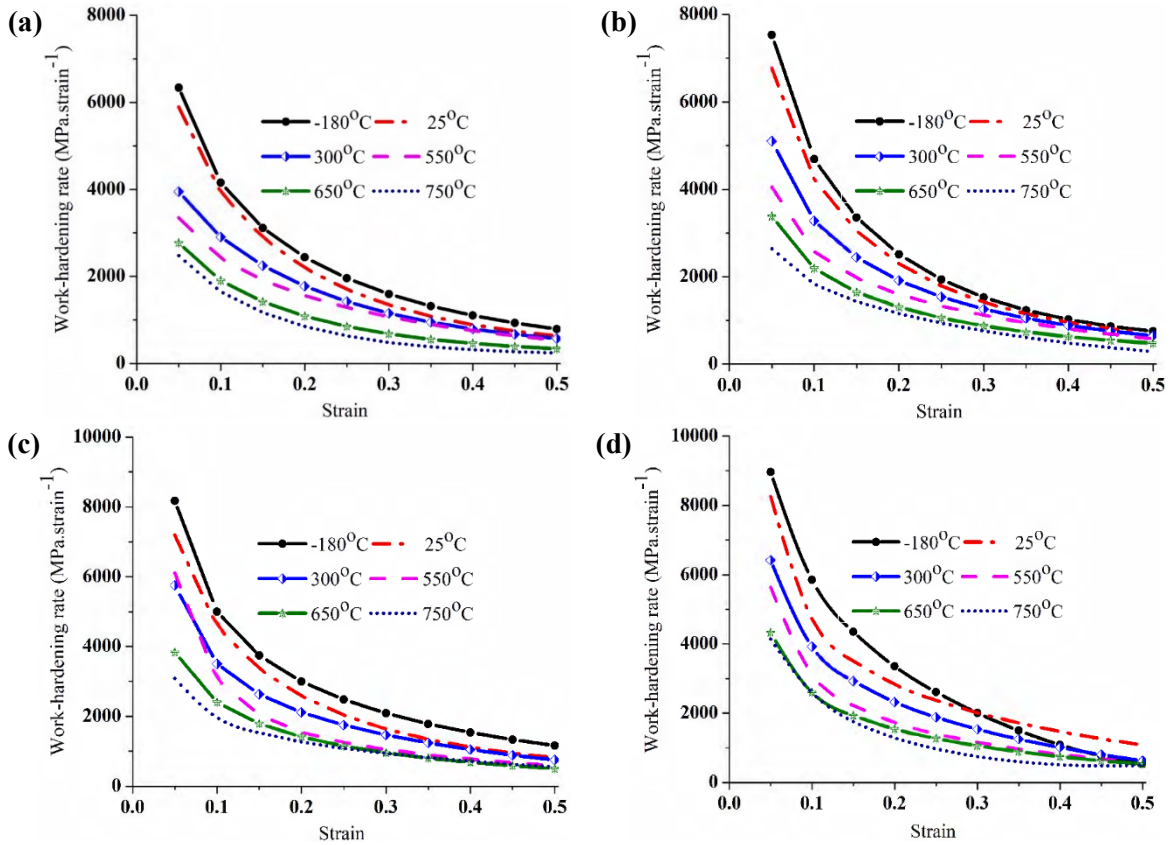

Figure 12. Work-hardening rate of NPH-718 alloy (a, b, c and d) at constant strain, strain rates ($4 \times 10^3\ s^{-1}$ to $7.5 \times 10^3\ s^{-1}$) and different temperatures (-180℃ to 750ºC).

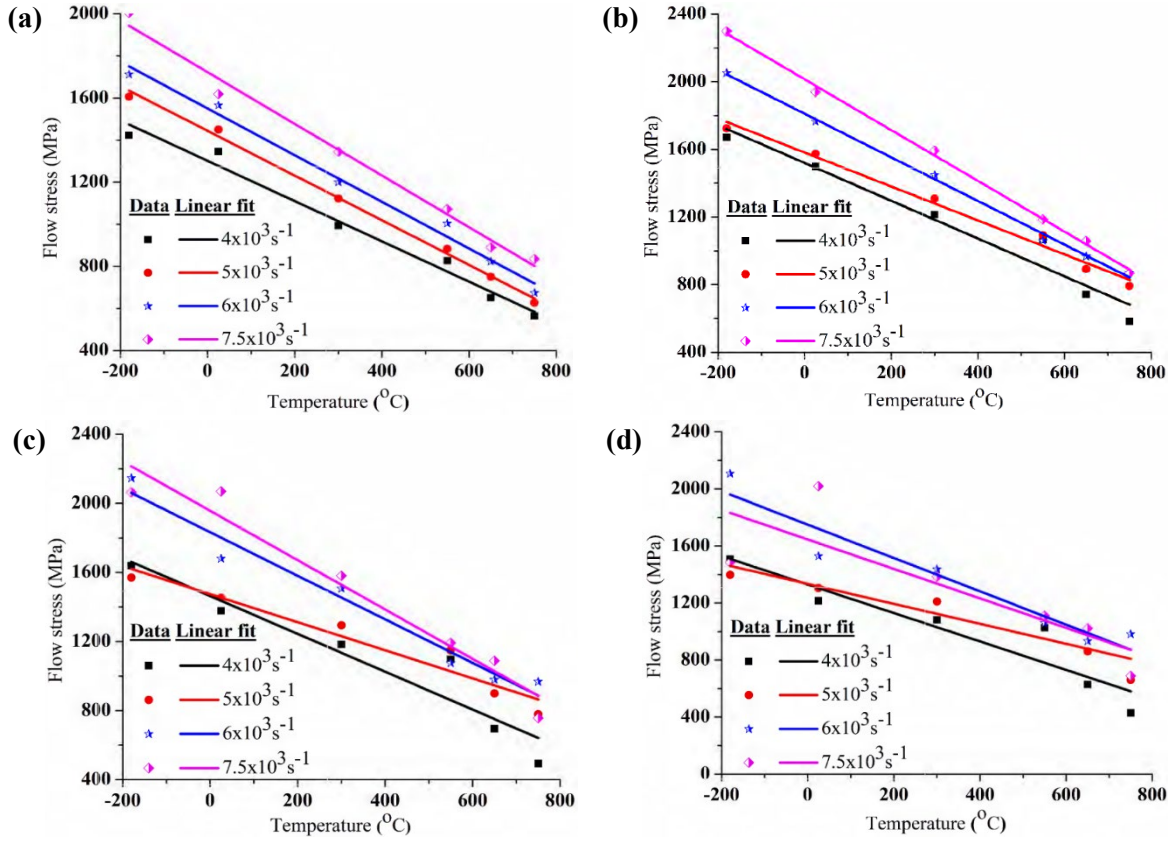

Figure 13. Dependency of flow stress of NPH-718 alloy on temperature as a function of constant strains: (a) 0.1, (b) 0.2, (c) 0.3, and (d) 0.4, at varied strain rate: 4×10^3 to $7.5 \times 10^3\ s^{-1}$.

3.7 Materials' sensitivity of NPH-718 alloy

Flow stress of materials under dynamic impact deformation could be dependent on some key influential deformation parameters. In other words, this implies that a material under deformation could have increase in flow stress as well as increase in those parameters. Moreover, the reverse trend could also be the resultant situation. Thus, the evaluation of the dynamic flow stress sensitivity of NPH-718 alloy to temperature as well as strain rate is of essence.

3.7.1 Effect of temperature on flow stress (temperature sensitivity)

The dynamic flow behaviour of the NPH-718 alloy under constant strain rate highlights the significant effect of deformation temperature on the dynamic response of the superalloys examined in this study. The results reported in Figure 13 clearly demonstrate the substantial link between flow stress and deformation temperature over the full range of plastic strain values and strain rates, particularly within the plastic strain range of 0.1 to 0.3 and strain rate from $4 \times 10^3\ s^{-1}$ to $7.5 \times 10^3\ s^{-1}$, which indicate that as the deformation temperature increases, there is a resultant and significant decrease in the resistance of the flow stress. This conforms to the assertion of [27]. Evidently, the decrease in the flow stress resulting from an increased temperature suggests that NPH-718 alloy studied is temperature dependent or sensitive. Thus, the dependency of the temperature effect with regards to the plastic strain, deformation temperature and strain rate can be evaluated using the temperature sensitivity parameter β_{Temp} defined in Equation (7)

$$\beta_{Temp} = |ln[\sigma_2\text{-}\sigma_1]/ln[T_2\text{-}T_1]| \quad (7)$$

Where σ_2, σ_1 represent the corresponding true stresses of tests conducted under the same strain rates at constant temperatures T_2, T_1 respectively with T_1 as 25°C. Obviously, β_{Temp} differs to some little extent with the plastic strain for the range of temperatures considered in this study. As a result, the influence of plastic strain can be ignored. Thus, the average value of temperature sensitivity is considered for analysis across the temperature ranges at various strain rate conditions.

Figure 14 (a-c) show the average temperature sensitivity (β_{Temp}) of the examined specimens in terms of strain rate at various temperatures. It is worth noting that, for a given temperature, β_{Temp} decreases as the strain rate increases. β_{Temp}, on the other hand, rises as the temperature rises, keeping the strain rate constant. This discovery suggests that at higher temperatures, the overall temperature rise or heat created during the plastic deformation process, which represents the rate of thermal softening, is more pronounced. Furthermore, Figure 14(a-c) compare the temperature sensitivity of alloys, with IN718 having a significantly higher β_{Temp} value. In conclusion, the temperature sensitivity findings in this work support the hypothesis that deformation temperature largely influences the mechanical response of the NPH-718 alloy, especially at high strain rates. This is consistent with earlier findings [5].

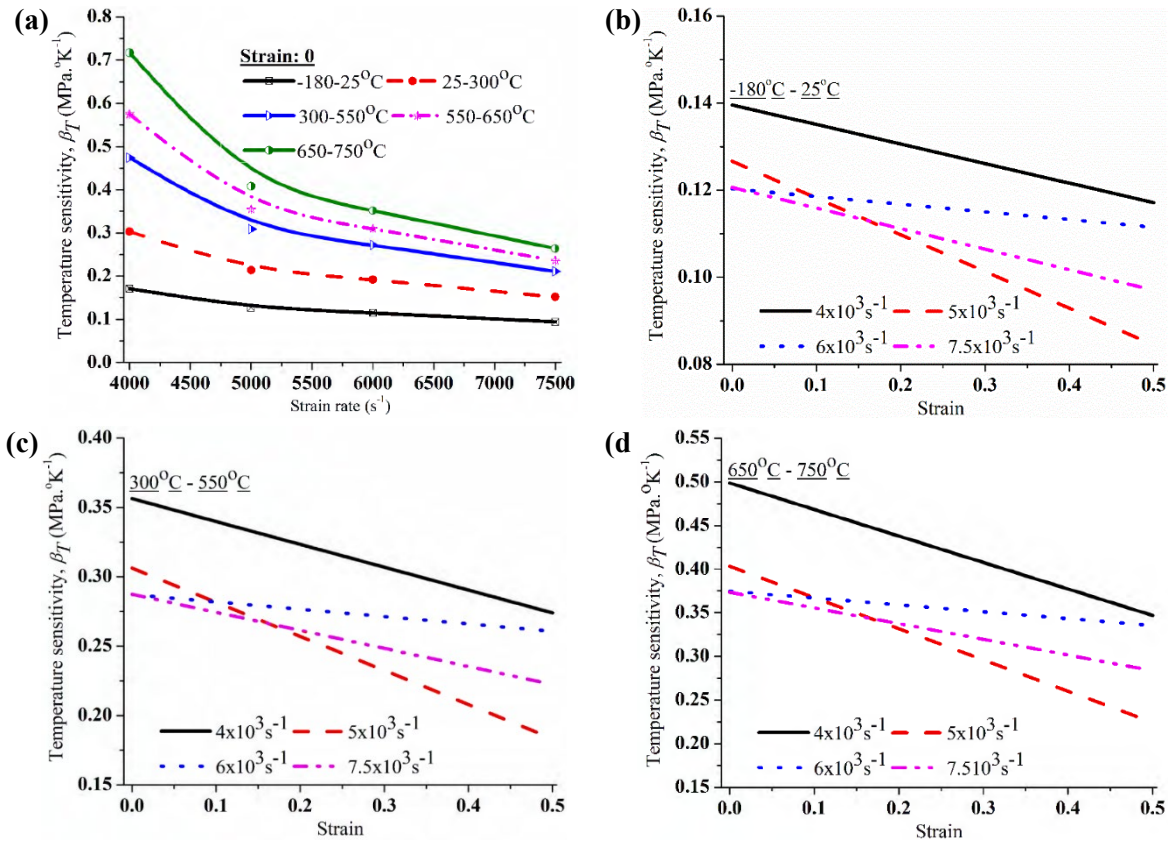

Figure 14. Variation of temperature sensitivity of NPH-718 alloy at constant strain: (a) 0.1, (b) 0.2, (c) 0.3, and (d) 0.4.

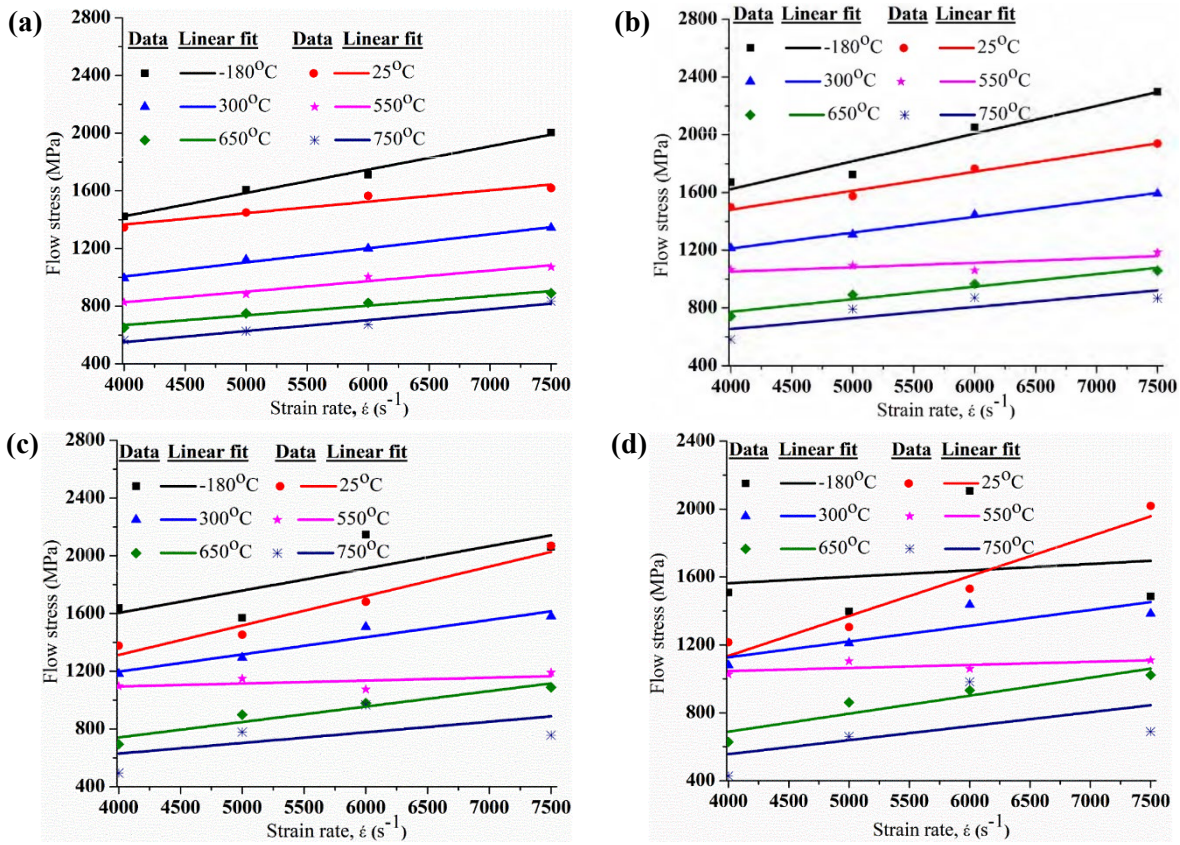

Figure 15. Dependency of flow stress on strain rate as a function of different strains: (a) 0.1, (b) 0.2 and (c) 0.3, and strain rates.

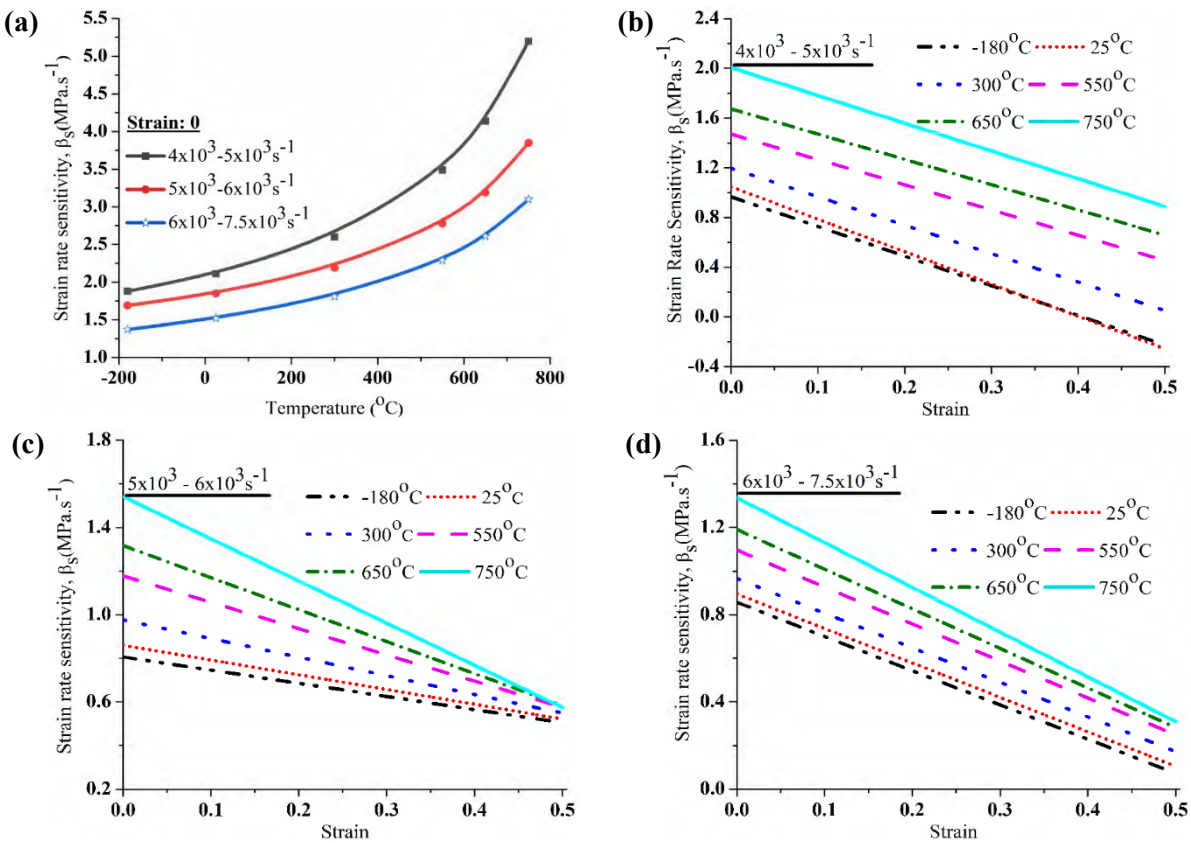

Figure 16. Variation of Strain rate sensitivity of NPH-718 alloy at strain: (a) 0.1, (b) 0.2, (c) 0.3 and (d) 0.4; and different temperatures (–180℃ to 750℃).

3.7.2 Effect of strain rate on flow stress (strain rate sensitivity)

The interplay between strain rate sensitivity and the strain rate of the investigated alloys in this study can be elucidated through the plotting of yield stress variation against strain rate at a specific plastic strain. As demonstrated in Figure 9(a-c), the yield stress experiences a decline with an increase in temperature under constant conditions of plastic strain and strain rate. These alloys have a high sensitivity to strain rate variations, which increases with greater strain rates while keeping a constant temperature and plastic strain. Figure 14(a-c) depicts the variation in strain rate sensitivity among the nanoprecipitation-hardened alloys under consideration. It is worth mentioning that the strain rate sensitivity of the studied samples increases with the plastic strain for all evaluated plastic strains. This noticeable increase in strain rate sensitivity can be attributed to an increased effect of the dislocation resistance mechanism at higher loading rates. This enhanced strain rate sensitivity may result from an increased rate of dislocation creation, an increased rate of martensite transition, or a proclivity for the immediate development of twin structures at higher strain rates [28]. The strain rate sensitivity parameter in Equation (8) may be used to completely examine the strain rate effect and its dependence on temperature and strain rate:

$$\beta_{ST} = |ln[\sigma_2\text{-}\sigma_1]/[\dot{\varepsilon}_2\text{-}\dot{\varepsilon}_1]| \quad (8)$$

where σ_2 and σ_1 are the respective compressive stresses resulting from impact tests carried out at average strain rates of $\dot{\varepsilon}_2$ and $\dot{\varepsilon}_1$. The variation of the strain rate sensitivity of the NPH-718 alloy against the deformation temperature with respect to strain rate and plastic strain are presented in Figure 15 (a-d).

Thus, the processes involved in dynamic deformation are controlled by deformation mechanism that are thermally activated in the region of high strain rate under the influence of the activation volume, $v^*$and energy, Q [29]. These deformation mechanisms are directly related to the flow stress and the strain rate are expressed in Equations (9-11).

$$\dot{\varepsilon} = \dot{\varepsilon}_0 \times \exp\,[\text{-Q/kT}] \quad (9)$$

$$v^* = T \times k \times [\partial\, ln\, \dot{\varepsilon}/\partial\sigma]_T \quad (10)$$

$$\text{Q} = v^* \times T \times [\partial\sigma/\partial\text{T}]_{\dot{\varepsilon},\,\varepsilon} \quad (11)$$

Where $\dot{\varepsilon}, \dot{\varepsilon}_0, Q, k, T, v^* and\ \sigma$ are the strain rate, frequency factor, activation energy, Bolzmann constant, absolute deformation temperature, activation volume and flow stress respectively. In a similar manner to temperature sensitivity, the value of dynamic strain rate sensitivity parameter (Figure 16(a-d) for NPH-718 alloy is remarkably high virtually in all the high loading conditions considered in this study. The findings reveal a direct correlation between the alloy's strain rate sensitivity, increasing strain rate, and plastic strain. As both strain rate and plastic strain intensify, the strain rate sensitivity exhibits a corresponding increase. Conversely, as the deformation temperature escalates, there is a noticeable decrease in the strain rate sensitivity. Of particular note is the significant reduction in strain rate sensitivity, especially pronounced at higher strain rates within the studied temperature range, ranging from $5 \times 10^3\ s^{-1}$ to $7.5 \times 10^3\ s^{-1}$. This rapid decline in the strain rate sensitivity parameter's value at elevated temperatures is attributed to the increased deformation, resulting in a rise in temperature.

4. Conclusion

In summary, this study successfully engineered NPH-718 alloy with nanoprecipitates of approximately 19 nm size using a meticulously controlled process that included extended heat treatment phases (solutionization, stabilization, and precipitation hardening) followed by controlled cooling.

Notably, NPH-718 alloy has demonstrated a robust dynamic response within a specified strain rate range ($4 \times 10^3\ s^{-1}$ to $7.5 \times 10^3\ s^{-1}$) and a broad temperature range (–180°C to 750°C), making it well-suited for applications with high dynamic impact deformations. This study not only produced a significant dataset on the dynamic deformation behaviour of NPH-718 alloy, but it also produced insights that are applicable to a variety of circumstances, including documentation, finite element analysis (FEA), and design concerns. It is critical to note that the produced alloys exhibit a significant thermal activation response under dynamic impact loading conditions, with the rate of thermal softening and strain rate sensitivity being much higher at higher temperatures and stresses, respectively. However, at higher deformation temperatures, the strain rate sensitivity decreases, highlighting the complex interaction of temperature and strain rate sensitivity in NPH-718 alloy. This highlights the alloy's complex sensitivity to temperature and strain rate, an important aspect for future study and applications.

Acknowledgements

The superalloy samples, technical expertise, laboratory facilities, reagents, equipment, and machinery utilized in this research were generously provided by Professor Olanrewaju A. Ojo and his research team from the Mechanical Engineering Department at the University of Manitoba, Canada. The authors extend their sincere appreciation for their invaluable support.

References

[1] H. J. Penkalla, J. Wosika, and A. Czyrska-Filemonowicz, "Quantitative microstructural characterization of Ni-base superalloys." *Materials Chemistry and Physics*, vol. 81, no. 2-3, pp. 417-423, 2003.

[2] P. K. Sarkar, R. Ghosal, P. Rao, and V. G. Kumar, "High temperature low cycle fatigue behaviour of hot isostatically pressed superalloy Udimet 720 LI." *Materials at High Temperatures*, vol. 27, pp. 295-300, 2010.

[3] M. K. Sinha, R. Madarkar, S. Ghosh, and V. R. Paruchuri. "Some investigations in grindability improvement of Inconel 718 under ecological grinding," *Proceedings of the Institution of Mechanical Engineers, Part B: Journal of Engineering Manufacture,* vol. 233, no. 3, pp.727-744, 2019.

[4] Y. Wang, W. Z. Shao, L. Zhen, L. Yang, and X. M. Zhang, "Flow behaviour and microstructures of superalloy 718 during

high temperature deformation," *Materials Science and Engineering: A*, vol. 497, no. 1-2, pp. 479-486, 2008.

[5] W-S. Lee, C-F. Lin, T-H. Chen, and H-W. Chen, "Dynamic impact response of inconel 718 alloy under low and high temperatures," *Materials Transactions*, vol. 52, no. 9, pp. 1734-1740, 2011.

[6] P. H. Pope, and J. E. Field, "Determination of strain in a dynamic compression test," *Journal of Physics E: Scientific Instruments*, vol. 17, no. 9, pp. 817-820, 1984.

[7] D. A. Gorham, P. H. Pope, and J. E. Field, "An improved method for compressive stress-strain measurements at very high strain rates." *Proceedings of the Royal Society A: Mathematical, Physical and Engineering sciences,* vol. 438, no. 1902, pp. 153-170, 1992.

[8] N. A. Fleck, M. P. F. Sutcliffe, S. Sivashanker, and X. J. Xin, "Compressive R-curve of a carbon fibre-epoxy matrix composite," *Composites Part B: Engineering*, vol. 27, no. 6, pp. 531-541, 1996.

[9] W. G. Ferguson, A. Kumar, and J. E. Dorn, "Dislocation damping in aluminum at high strain rates," *Journal of Applied Physics*, vol. 38, 1863-1869, 1967.

[10] A. Seeger, "The generation of lattice defects by moving dislocations, and its application to the temperature dependence of the flow-stress of F.C.C. crystals," *The London, Edinburgh, and Dublin Philosophical Magazine and Journal of Science*, vol. 46, no. 382, pp. 1194-1217, 1955.

[11] K. Ogawa, and T. Nojima, "Impact strength of titanium alloys," *Journal of the Society of Materials Science, Japan,* vol. 37, no. 421, 1171-1177, 1988.

[12] W. S. Lee, and C. F. Lin, "High-temperature deformation behaviour of Ti6Al4V alloy evaluated by high strain-rate compression tests," *Journal of Materials Processing Technology,* vol. 75, no. 1-3, pp. 127-136, 1998.

[13] C. Y. Chiem, and J. Duffy, "Strain rate history effects and observations of dislocation substructure in aluminum single crystals following dynamic deformation," *Materials Science and Engineering*, vol. 57, pp. 233-247, 1983.

[14] L. Martin, "The Theory of the microscope - IV: The boundary-wave theory of image formation," *Proceedings of the Physical Society, Section B,* vol. 62, no. 11, pp. 713-725, 1949.

[15] O. A. Idowu, O. A. Ojo, and M. C. Chaturvedi, "Crack-free electron beam welding of Allvac 718Plus® superalloy," *Welding Journal, (Miami Fla),* vol. 88, pp. 179s-187s, 2009.

[16] J. Delorme, "Extension of a finite element model to 2D for the prediction of adiabatic shear bands," M.Sc. Thesis in Mechanical Engineering at the University of Manitoba, Canada, Manitoba, 2012.

[17] W.-S. Lee, C.-F. Lin, T.-H. Chen, and H.-W. Chen, "dynamic impact response of inconel 718 alloy under low and high temperatures," *Materials Transactions,* vol. 52, no. 9, pp. 1734-1740, 2011.

[18] J. T. (B.S.) Hammer, "Plastic deformation and ductile fracture of Ti-6Al-4V under various loading conditions," M.Sc. Degree Thesis in Mechanical Engineering at the Ohio State University, 2012.

[19] Y. Wang, W.Z. Shao, L. Zhen, L. Yang, and X. M. Zhang, "Flow behavior and microstructures of superalloy 718 during high temperature deformation," *Materials Science and Engineering A*, vol. 497, pp. 479-486, 2008.

[20] S.-T. Chiou, H.-L. Tsai, and W.-S. Lee, "Effects of strain rate and temperature on the deformation and fracture behaviour of titanium alloy," *Materials Transactions*, vol. 48, no. 9, pp. 2525-2533, 2007.

[21] C. I. Garcia, G. D. Wang, D. E. Camus, E. A. Loria, and A. J. DeArdo, "Hot deformation behavior of superalloy 718," Proceedings of the international symposium on superalloys 7X3,625,706 and various derivatives, The Minerals, Metals and Materials Society, E. A. Loria, ed., pp. 293-302, 1994.

[22] G.-Z. Quan, W.-Q. Lv, Y.-P. Mao, Y.-W. Zhang, and J. Zhou, "Prediction of flow stress in a wide temperature range involving phase transformation for as-cast Ti–6Al–2Zr–1Mo–1V alloy by artificial neural network," *Material Design,* vol. 50, pp. 51-61, 2013.

[23] H. Onovo, D. Esezobor, and M. Bodude, "Dynamic impact response of nanosized precipitates bearing waspaloy." *The Journal of Engineering Research [TJER],* vol. 19 no. 2, pp. 180-189, 2023.

[24] Y. Ashuach, Z. Rosenberg, and C. Avinadav, "Multi-step Kolsky bar loading of materials which fail by adiabatic shear banding," *Journal of Physics, Conference Series*, 500, 2014.

[25] D. MacDougall, "Determination of the plastic work converted to heat using radiometry," *Experimental Mechanics*, vol. 40, no. 3, pp. 298-306, 2000.

[26] C. Fichera, "High strain-rate and temperature behaviour of metals: Advanced testing and modelling," Ph.D. Thesis, Politecnico di Torino (Polytechnic University of Turin), Italy, Turin, 2015.

[27] W.-S. Lee, C.-Y. Liu, and T.-N. Sun, "Dynamic impact response and microstructural evolution of inconel 690 superalloy at elevated temperatures," *International Journal of Impact Engineering,* vol. 32, pp. 210-223, 2005.

[28] W.-S. Lee, and C. F. Lin, "Comparative study of the impact response and microstructure of 304L stainless steel with and without prestrain," *Metallurgical and Materials Transactions A,* vol. 33, no. 9, pp. 2801-2810, 2002.

[29] W.-S. Lee, T.-H. Chen, C.-F. Lin, and Z.-Y. Li, "Effects of strain rate and temperature on shear properties and fracture characteristics of 316L stainless steel," *Materials Transactions*, vol. 53, no. 3, pp. 469-476, 2012.